

Solar Field and Receiver Model Validation of the Next-CSP MW-Scale Prototype

Benjamin Grange ¹, Alex Le Gal ¹, and Gilles Flamant ^{1,*}

¹ PROMES-CNRS, 66120 Font Romeu, France

*Correspondence: Gilles Flamant, gilles.flamant@promes.cnrs.fr

Abstract. This study presents a comparison of both modelling and experimental results obtained on the solar field and the receiver of the MW-scale particle driven CSP unit implemented at the Themis solar tower (France) in the framework of the Next-CSP H2020 European project. At partial load, ~900 kW, the simulated data concerning the incident power at the receiver aperture are consistent with the measured values with less than 5% difference from the experimental results. The difference is higher for the particle temperature and the thermal efficiency as a function of particle mass flow rate. It ranges between 12 and 98°C for measured particle temperature of 430 and 300°C respectively. For the thermal efficiency, the difference varies strongly with the experiments from approximately 12% to 50% (relative). The main cause of discrepancy between the experimental and the calculated results is attributed to the heterogeneity of the solar flux distribution on the receiver tubes.

Keywords: Solar Field, Central Receiver, Modelling, Measurements, Particle-driven CSP

1. Introduction

Several leading research projects are currently dedicated to particle-based CSP technology [1]. The falling particles receiver has been conceptualized and developed by the SANDIA national laboratory (SNL) in the USA [2]. In this concept, particles directly absorb the concentrated solar radiations during their fall at the focus of the heliostat field. Ho et al. reported test results of a 1MW_{th} falling particle receiver obtained using the 5 MW_{th} SNL solar tower facility in Albuquerque [3]. The centrifugal particle receiver concept developed by DLR in Germany was first demonstrated at lab-scale [4] and a MW-scale solar receiver was designed and tested at partial load at the DLR's test facility Jülich Solar Tower [5]. A solar receiver using particles flowing down in transparent tubes has been tested at Badaling Concentrated Solar Power Tower at the MW-scale [6]. In the fluidized particles-in-tube solar receiver concept developed by CNRS, fluidized particles move upward into vertical metallic tubes that are irradiated by concentrated solar radiations. The particles flowrate inside the tubes is controlled via a pressure drop imposed between the inlet and outlet of the receiver tube. Small size (<100 μm) silicon carbide and olivine particles have been used to achieve high tube wall-to-particle heat transfer coefficients. A MW-scale solar receiver was implemented at the Themis solar tower (France) in the framework of the Next-CSP H2020 European project [7]. This paper presents a comparison of the results of both modelling and experimental works on the solar field and the receiver.

2. The Next-CSP prototype and instrumentation

The MW-scale particle loop implemented at the Themis solar tower is composed of four principal elements that are the cold store, the solar receiver (40, 4m-long tubes), the hot store and the heat exchanger. All the components are located at the tower top (focal area). The solar field of Themis consists of 107 heliostats. Each heliostat is 54 m². For the first experimental campaign, a maximum of 24 heliostats was considered. Figure 1 shows the solar receiver in operation. A length of 3 m from the 4 m is irradiated by concentrated solar energy (the irradiated part size is 3 m high and 2.6 m wide). Each tube of the receiver is made of two sections, eight fins are welded inside each tube along 2 m, from 1 meter to 3 meters high, to improve heat transfer, the first meter is a bare tube [8].

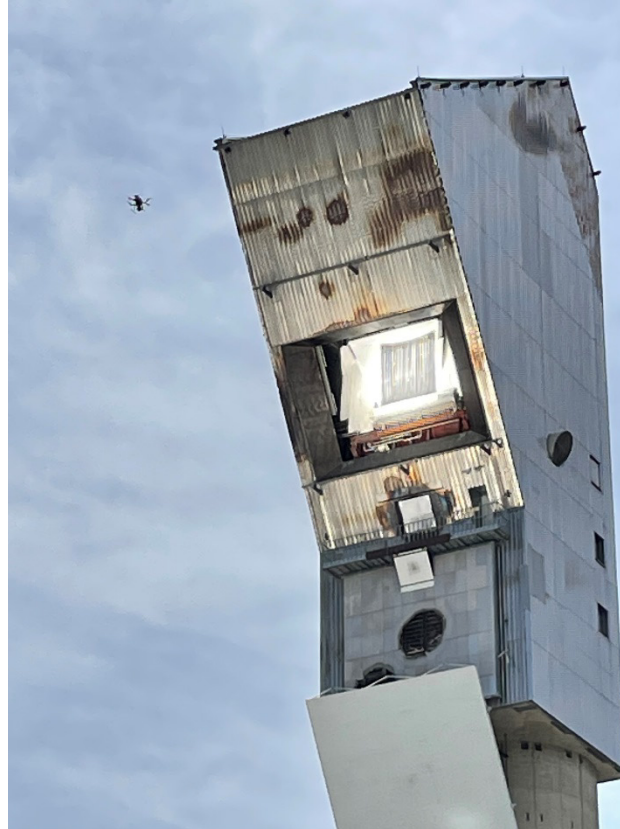


Figure 1. The MW-scale fluidized bed solar receiver in operation

The loop has been fully equipped with temperature sensors, pressure probes, flowmeters and automated valves to measure the key parameters that control the particles circulation (mass flowrate) and characterize the solar receiver thermal behaviour. At Themis facility, the flux measurement system consists of a white moving bar, a radiometer installed on the moving bar and a digital camera. The white moving bar is a diffuse surface that reflects the concentrated radiation that is captured by the digital camera. The moving bar crosses the aperture of the receiver while the digital camera is taking high FPS pictures. These pictures are matrixes of numbers in units of Grey Level (GL) or brightness.

3. The modelling approach and validation

3.1 Heliostat field and solar receiver modelling

The heliostat field is modelled using Solstice, an open-source ray-tracing software developed by the CNRS-PROMES laboratory and Meso-Star SAS [9]. Solstice uses the YAML language (Yet Another Markup Language) to create geometries. It is designed to handle efficiently

complex solar facilities. CAD model can be imported and therefore complex ray's path can be simulated. The influence of the variation of surface optical properties with wavelength can also be taken into account.

The flux distribution on each tube of the solar receiver computed by Solstice is post-processed and considered in a simplified thermal model developed with the Matlab® software. The thermal model is based on the Net Radiation Method, which establishes the balance on heat flux and radiosity. The discretization of the tubes for the thermal model is performed by dividing each of them into 15 parts in height, and considering the front and the back of the tube. This discretization results in 1200 elements for the forty tubes (30 elements per tube). Details can be found in [10].

3.1.1. Solar power and flux distribution at the receiver aperture

Figure 2 illustrates a flux distribution map at the receiver aperture for 24 heliostats focusing concentrated solar radiation at the bottom center of the receiver, resulting in a maximum flux density of $275 \text{ kW}\cdot\text{m}^{-2}$. The corresponding incident power normalized for a DNI of $1000 \text{ W}/\text{m}^2$ is $890 \pm 90 \text{ kW}$. The simulated data concerning the incident power are consistent with the measured values with less than 5% difference from the experimental results.

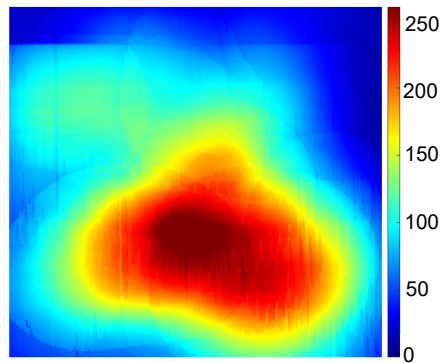


Figure 2. Example of measured flux density distribution ($\text{kW}\cdot\text{m}^{-2}$)

3.1.2. Particle temperature and receiver thermal efficiency

The set of experimental runs taken into account for this comparison is listed in Table 1.

Table 1. Operation conditions of the set of experimental runs

| Run | Particle mass flowrate (kg/h) | Particle mass flowrate (kg/s) | Solar Power (kW) | T _{part,in} (°C) |
|-----|-------------------------------|-------------------------------|------------------|---------------------------|
| 1 | 2148 | 0,60 | 719 | 38 |
| 2 | 3260 | 0,91 | 783 | 30 |
| 3 | 3985 | 1,11 | 783 | 30 |
| 4 | 4435 | 1,23 | 653 | 19 |
| 5 | 9972 | 2,77 | 553 | 23 |
| 6 | 12456 | 3,46 | 542 | 28 |

Concerning the thermal model of the solar receiver, the following assumption have been made. The solar flux distribution on the tube surface is the same for the 40 elements of the receiver. It is plotted in Figure 3. The flux density is maximum at 1 m, as in the experiments, since this location corresponds to the beginning of the finned tube section.

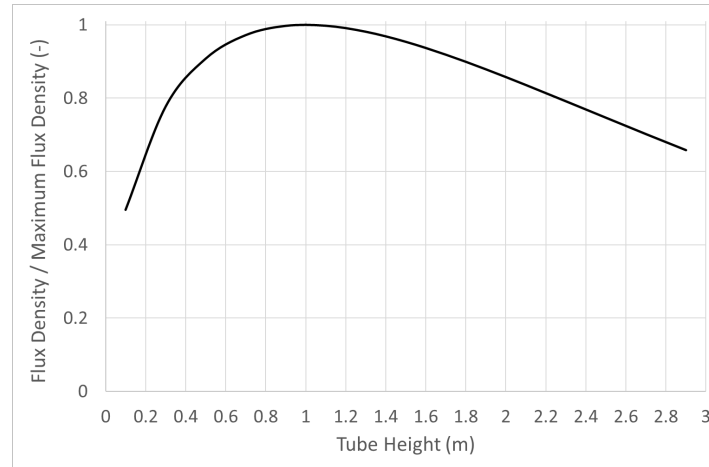


Figure 3. Assumed non dimensional vertical solar flux distribution in the model

Table 2 and Table 3 compare the experimental and calculated data for the particle temperature and the receiver thermal efficiency respectively.

Table 2. Comparison of experimental and measured mean particle outlet temperature

| Run | T _{part,in} (°C) | T _{part,out} (°C) <i>Measured</i> | T _{part,out} (°C) <i>Calculated</i> |
|-----|---------------------------|-----------------------------------------------|-------------------------------------------------|
| 1 | 38 | 442 | 492 |
| 2 | 30 | 430 | 442 |
| 3 | 30 | 300 | 398 |
| 4 | 19 | 250 | 314 |
| 5 | 23 | 142 | 149 |
| 6 | 28 | 113 | 128 |

Table 3. Comparison of experimental and measured power transferred to the particles and receiver thermal efficiency

| # | Solar Power (kW) | P _{part} (kW) <i>Measured</i> | P _{part} (kW) <i>Calculated</i> | Thermal efficiency (%) <i>Measured</i> | Thermal efficiency (%) <i>Calculated</i> |
|---|------------------|-------------------------------------------|---------------------------------------------|-------------------------------------------|---------------------------------------------|
| 1 | 719 | 253 | 311 | 35,2 | 43.3 |
| 2 | 783 | 380 | 429 | 48,6 | 54.7 |
| 3 | 783 | 314 | 468 | 40,1 | 59.8 |
| 4 | 653 | 299 | 418 | 45,8 | 64 |
| 5 | 553 | 346 | 403 | 62,6 | 72.8 |
| 6 | 542 | 309 | 397 | 57,0 | 73.3 |

Figures 4 and 5 plot the compared experimental and calculated results from the data listed in the previous Tables.

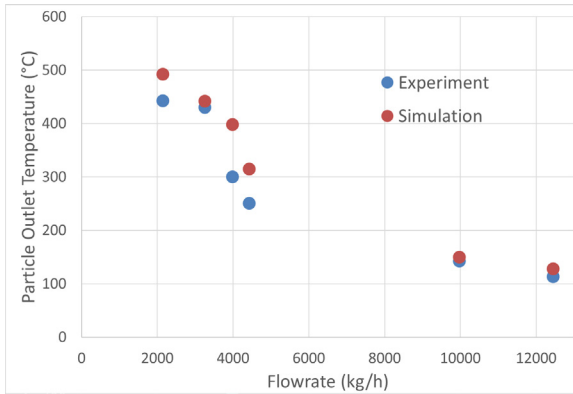


Figure 4. Comparison of the outlet particle temperature

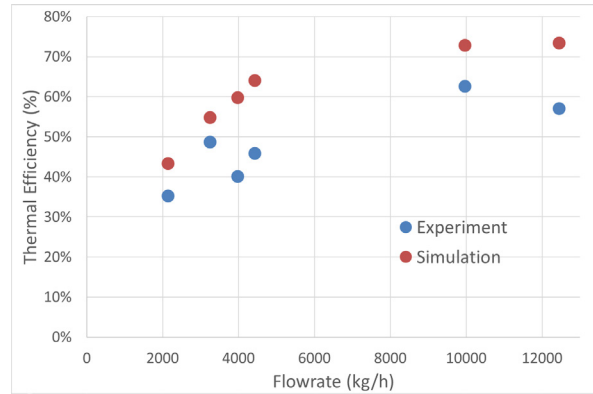


Figure 5. Comparison of the receiver thermal efficiency

The comparison arouses three remarks:

- The trends are similar for both experimental and calculated data;
- The agreement between the measured and the calculated data for the particle temperature is better than for the thermal efficiency;
- Concerning the thermal efficiency, the difference varies strongly with the experiments from approximately 12% to 50% (relative).

Apart the experimental uncertainties ($\pm 20\%$), the main cause of discrepancy between the experimental and the calculated results is the heterogeneity of the solar flux distribution on the receiver tubes. It is assumed homogeneous on the 40 tubes (with the vertical distribution plotted in Figure 3) in the model since it is not during the experimental runs. This heterogeneity results in variations of particle mass flow rate between the tubes and local overheating of the tube walls.

3.1.3. Additional data from the thermal model

The model enables predicting the evolution of the tube and particle temperatures along the tube height. Figure 6 illustrates the calculated front tube wall and particle temperature variation with tube height for two extremum particle mass flow rate, low (0,60 kg/s) and high (3.46 kg/s).

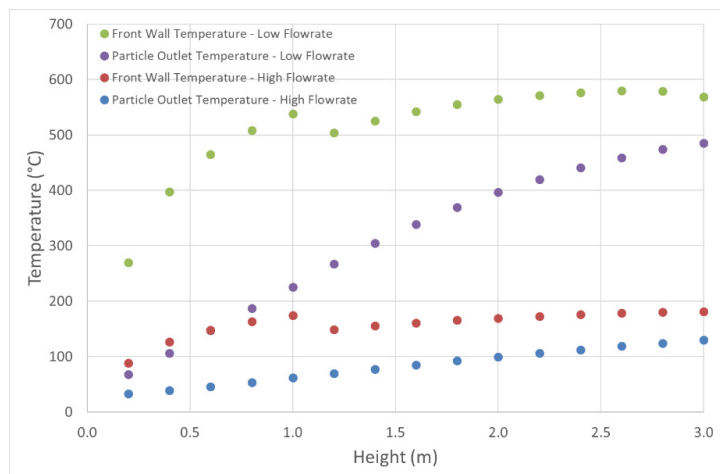


Figure 6. Calculated tube wall and particle temperature profiles for the minimum and maximum particle mass flow rates (see Table 1)

On the tube wall temperature profile, the slope variation at 1 m corresponds to the boundary between the bare and the finned tube sections in which two values of the global heat transfer coefficient were applied. These values are 350 and 500 W/m².K for the bare and the finned tube sections respectively. They are not the wall-to-fluidized bed heat transfer coefficient but the global coefficient accounting for conduction in the tube wall and the internal heat exchange. For the low particle mass flow rate, temperature difference between the wall and the particle as large as 300°C are predicted. It is reduced to 120 °C for high mass flow rate. At the outlet, the difference is less than 100°C and ~50°C respectively.

4. Conclusion

This paper presents a comparison of both modelling and experimental data of a MW-scale solar receiver including solar flux distribution at the aperture, radiation distribution inside the solar receiver half-cavity and heat transfer to the fluidized particles. At partial load, it is shown that despite a good agreement concerning the flux distribution, the particle temperature and the thermal efficiency show larger differences due to flux distribution heterogeneity on the receiver tubes. This indicates that the thermal model must be improved to account for partial load operation modes with heterogeneous distribution of the solar flux on the solar receiver tubes.

Data availability statement

The data can be accessed by direct query to the authors.

Author contributions

Benjamin Grange: modelling and software, data curation, writing – review & editing; Alex Le Gal: data curation, investigation, writing – review & editing; Gilles Flamant: funding acquisition, supervision, validation, writing – original draft.

Competing interests

The authors declare that they have no competing interests.

Funding

This work has received funding from the European Union's Horizon 2020 research and innovation program under grant agreement No 727762, Next-CSP project.

Acknowledgement

The authors thanks Marina Casanova, Antoine Perez, William Baltus and Mickaël Tessonnaud for their contribution to the experimental campaign.

References

1. Flamant, G., Grange, B., Wheeldon, J., Siros, F., Valentin, B., Bataille, F., Zhang, H., Deng, Y., Baeyens, J. Opportunities and challenges in using particle circulation loops for concentrated solar power applications. *Progress in Energy and Combustion Science* 94, 101056, 2023. <https://doi.org/10.1016/j.pecs.2022.101056>

2. Martin J, Vitko J., ASCUAS: a solar central receiver utilizing a solid thermal carrier. 1982. Albuquerque, NM, and Livermore, CA (United States): <https://doi.org/10.2172/5663779>
3. Ho CK, Christian JM, Yellowhair J, Armijo K, Kolb WJ, Jeter S, et al. Performance Evaluation of a High-Temperature Falling Particle Receiver. Vol. 1 Biofuels, Hydrog. Syngas, Altern. Fuels; CHP Hybrid Power Energy Syst. Conc. Sol. Power; Energy Storage; Environ. Econ. Policy Considerations Adv. Energy Syst. Geothermal, Ocean. Emerg. E, American Society of Mechanical Engineers, 2016. <https://doi.org/10.1115/ES2016-59238>
4. Wu W, Trebing D, Amsbeck L, Buck R, Pitz-Paal R. Prototype Testing of a Centrifugal Particle Receiver for High-Temperature Concentrating Solar Applications. *J Sol Energy Eng*, 137(4): 041011, 2015. <https://doi.org/10.1115/1.4030657>
5. Ebert M, Amsbeck L, Rheinländer J, Schlögl-Knothe B, Schmitz S, Sibum M, et al. Operational experience of a centrifugal particle receiver prototype, AIP Conference Proceedings 2126, 030018., 2019. <https://doi.org/10.1063/1.5117530>
6. Yu Y, Hu F, Bai F, Wang Z. On-sun testing of a 1 MWth quartz tube bundle solid particle solar Receiver. *Renewable Energy*, 193, 383-397, 2022. <https://doi.org/10.1016/j.renene.2022.05.036>
7. Le Gal A, Grange B, Casanova M, Perez A, Baltus W, Tessonnaud M, Flamant G. Experimental results of the MW-scale fluidized particle-in-tube solar receiver first test campaign. *Solar Energy* 262, 111907, 2023. <https://doi.org/10.1016/j.solener.2023.111907>
8. Le Gal A, Grange B, Tessonnaud M, Perez A, Escape C, Sans J-L, Flamant G. Thermal analysis of fluidized particle flows in a finned tube solar receiver. *Solar Energy* 191, pp. 19-33, 2019. <https://doi.org/10.1016/j.solener.2019.08.062>
9. PROMES-CNRS, MESO-STAR SAS. SOLSTICE, SOLar Simulation Tool In ConcEntrating optics, version 0.7.1 (2017) , France, <https://www.meso-star.com/projects/solstice.html> <https://www.labex-solstice.fr/logiciel-solstice.html>
10. Grange B. and Flamant G. Aiming Strategy on a Prototype-Scale Solar Receiver: Coupling of TABU Search, Ray-Tracing and Thermal Models. *Sustainability* 13, 3920, 2021. <https://doi.org/10.3390/su13073920>